

1 **The interaction between urbanization and aerosols during a typical winter haze**  
2 **event in Beijing**

3 Miao Yu<sup>1</sup>, Guiqian Tang<sup>2</sup>, Yang Yang<sup>1</sup>, Qingchun Li<sup>1</sup>, Yonghong Wang<sup>2</sup>, Shiguang  
4 Miao<sup>1</sup>, Yizhou Zhang<sup>1</sup>, Yuesi Wang<sup>2</sup>

5

6

- 7 1. *Institute of Urban Meteorology, China Meteorological Administration, Beijing, China*  
8 2. *State Key Laboratory of Atmospheric Boundary Layer Physics and Atmospheric Chemistry*  
9 *(LAPC), Institute of Atmospheric Physics, Chinese Academy of Sciences, Beijing 100029,*  
10 *China*

11

12

13

14

15 *Submitted to Atmospheric Chemistry and Physics*

16

17

18

19

20

21 *Corresponding author:*

22 **Guiqian Tang**

23 *State Key Laboratory of Atmospheric Boundary Layer Physics and Atmospheric Chemistry*  
24 *(LAPC), Institute of Atmospheric Physics, Chinese Academy of Sciences, Beijing 100029, China*

25

## Abstract

Aerosols cause cooling at the surface by reducing shortwave radiation, while urbanization causes warming by altering the surface albedo and releasing anthropogenic heat. The combined effect of the two phenomena needs to be studied in depth. The effects of urbanization and aerosols were investigated during a typical winter haze event. The event, which occurred in Beijing from 15-22 December 2016, was studied via the rapid-refresh multiscale analysis and prediction system-short term (RMAPS-ST) model. The mechanisms of the impacts of aerosols and urbanization were analyzed and quantified. Aerosols reduced urban-related warming during the daytime by 20% (from 30 to 50%) as PM<sub>2.5</sub> concentrations increased from 200 to 400  $\mu\text{g}\cdot\text{m}^{-3}$ . Conversely, aerosols also enhanced urban-related warming at dawn, and the increment was approximately 28%, which contributed to haze formation. Urbanization reduced the aerosol-related cooling effect by approximately 54% during the haze event, and the strength of the impact changed little with increasing aerosol content. The impact of aerosols on urban-related warming was more significant than the impact of urbanization on aerosol-related cooling. Aerosols decreased the urban impact on the mixing layer height by 148% and on the sensible heat flux by 156%. Furthermore, aerosols decreased the latent heat flux; however, this reduction decreased by 48.8% due to urbanization. The impact of urbanization on the transport of pollutants was more important than that of aerosols. The interaction between urbanization and aerosols may enhance the accumulation of pollution and weigh against diffusion.

## 1 Introduction

In recent years, heavy haze pollution events have increasingly occurred in densely populated urban areas, such as the Beijing-Tianjin-Hebei region (BTH region) and Yangtze River Delta region of China (Zhang et al., 2019). These events have caused increasingly severe adverse effects on transportation, the ecological environment and human health (Zhao et al., 2012; Wu et al., 2010; Liu et al., 2012). A statistical analysis of the variation in haze days in Beijing over the past 10 years showed that the number

55 of haze days has significantly increased (Chen and Wang, 2015; Zhai et al., 2019). The  
56 average annual number of haze days was 162 from 1981-1990, 167 from 1991-2000,  
57 and 188 from 2001-2010. The conditions for the formation of heavy haze in the BTH  
58 region are very complex (Miao et al., 2017; Wei et al., 2018; Ren et al., 2019). Although  
59 emissions, meteorological conditions, terrain, and high-density human activities in  
60 urban areas are all important conditions for the evolution of heavy haze (Huang et al.,  
61 2008a; Zhu et al., 2018), meteorological conditions are critical for the evolution of  
62 heavy haze pollution weather under the background of constant emissions (Wang et al.,  
63 2020; Pei et al., 2020).

64

65 The characteristics of the atmospheric boundary layer structure determine the  
66 horizontal fluidity, vertical diffusion ability, stability and capacity (mixed layer  
67 thickness) of the atmosphere, which are the main factors affecting the formation,  
68 intensity and duration of haze and atmospheric pollution (Guo et al., 2016). Coulter R  
69 L. (1979) indicated that the height of the mixing layer would affect the concentration  
70 and diffusion of pollutants, which has been one of the most important physical  
71 parameters in atmospheric numerical models and atmospheric environment evaluations,  
72 and urbanization and aerosols have been indicated to influence the boundary layer  
73 height (Tao et al., 2015).

74

75 Urbanization, as the most drastic means by which human activities transform the  
76 environment, has had an important impact on regional climate and weather processes  
77 (Miao et al., 2011; Yu and Liu, 2015; Yu et al., 2017). Existing research suggests that  
78 there are three main ways by which urbanization influences the climate (Oke, 1982 and  
79 1995). The change in land use from natural surfaces to impervious underlying surfaces  
80 in association with urbanization alters the surface albedo and roughness, which results  
81 in the formation of urban heat islands (UHIs) (Taha, 1997; Folberth et al., 2014). These  
82 alterations lead to a change in the surface energy balance and the form of the thermal  
83 difference between urban and rural areas and further change the boundary layer

84 structure (Grimmond, 2007; Li and Bou-Zeid, 2013). Second, thermal differences  
85 further lead to heat island circulation, which can influence the local circulation of  
86 synoptics and the transport of pollutants (Crutzen, 2004). Anthropogenic aerosols and  
87 heat from the development of transportation and industry are also important parts of  
88 urban impacts on climate (Huang et al. 2008b). However, in contrast to the effects of  
89 urbanization, aerosols cause cooling at the surface by reducing shortwave radiation to  
90 enhance static stability (Grimmond, 2007; Cruten, 2004, Huang et al., 2007).  
91 Furthermore, aerosols may increase longwave radiation in urban areas because they are  
92 likely to absorb and emit more energy than water vapor or greenhouse gases under  
93 certain conditions (Jacobson, 1998; Rudich et al., 2007). There have been few studies  
94 on the mechanism of the interaction between urbanization and aerosols, although many  
95 studies have focused on their respective effects. Accordingly, the interaction between  
96 urbanization and aerosols is important for studying regional climate.

97

98 Researchers are increasingly aware of the importance of the interaction between  
99 urbanization and aerosols. A very important study by Cao et al. (2016) describes the  
100 first attempt to determine the effects of aerosols on urbanization and indicated that  
101 aerosols can increase the nighttime UHI effect using a climate model. Yang et al. (2020)  
102 obtained different results when using observational data to perform similar research in  
103 the BTH region.

104

105 More detailed research needs to be performed by combining observational data and  
106 modeling because the conclusions may vary depending on the scale (Xu et al., 2019).  
107 Other illuminating work with regional models showed that the combined effect of UHIs  
108 and aerosols on precipitation depends on synoptic conditions (Zhong et al., 2015).  
109 However, for winter haze, Zhong et al. (2017) evaluated the impact of urban areas on  
110 air quality and indicated that urbanization can increase ventilation during the daytime  
111 and increase aerosol emissions, and these effects outweigh the UHI effect.

112

113 However, very few studies have quantified the individual effects of urbanization-  
114 induced UHIs and elevated aerosol emissions on the formation and development of  
115 haze in metropolitan areas. A difficulty faced by such studies is that the radiative forcing  
116 of aerosols is not a prognostic variable in most climate models (Cao et al. 2016). Some  
117 regional models, such as WRF-Chem, can overcome this problem by parameterizing  
118 aerosols to aerosol optical depth (AOD) in some specific radiation schemes. Tao et al.  
119 (2015) and Zhong et al. (2018) made some progress in this area, and their results also  
120 indicated that a regional model could be used as an effective way to study the interaction  
121 between urbanization and aerosols. However, a quantitative evaluation of the impacts  
122 of urban areas on aerosols and the simultaneous impacts of aerosols on urban impacts  
123 in metropolitan areas has not been attempted.

124

125 In this study, the rapid-refresh multiscale analysis and prediction system-short term  
126 (RMAPS-ST) was used to investigate the mechanism of the influence of the above two  
127 factors during a typical winter haze event. The objectives of this study are 1) to quantify  
128 the impacts of urban areas on aerosols and the impacts of aerosols on urbanization and  
129 2) to obtain a better understanding of the interaction between urbanization and aerosols  
130 and its influence mechanism on the boundary layer structure and haze transmission  
131 during a typical winter haze event in the BTH region.

132

## 133 **2 Methods**

### 134 **2.1 Observational data**

135 To investigate the interaction between urbanization and aerosols, observation data on  
136 basic meteorological elements, air quality, radiation and surface heat flux and the  
137 mixing layer height (MLH) are very important to reveal the impact of urbanization and  
138 aerosols during haze events.

139

140 The basic meteorological elements were obtained from 309 national basic weather  
141 stations in the BTH region and were provided by the China Meteorological

142 Administration (<http://data.cma.cn/>). The locations of the national basic weather  
143 stations are shown in Fig 1 (red dots). The mass concentrations of fine particulate matter  
144 (PM<sub>2.5</sub>) were recorded by 251 environmental monitor stations managed by the Ministry  
145 of Ecology and Environment of the People's Republic of China  
146 (<http://hbk.cei.cn/aspx/default.aspx>) (Fig 1, black dots). We also used radiation and  
147 surface heat flux data to analyze the urban surface energy budget obtained from the  
148 Beijing meteorological tower (39.97°N, 116.37°E). The tower is 325 m high and is  
149 operated by the Institute of Atmospheric Physics (IAP), Chinese Academy of Sciences  
150 (CAS). The heat flux data were measured by a fast response eddy covariance sensor  
151 system that was sampled at 10 Hz using CR500 (Campbell Scientific Inc., USA). The  
152 radiation data were provided by Kipp & Zonen (Netherlands) four-component  
153 unventilated CNR1 radiometers. Radiation and surface flux data from 140 m of the  
154 tower were used in this study. In addition, the MLH is an important factor affecting  
155 pollutant diffusion and is also affected by both urbanization and aerosols. Because the  
156 MLH is not a routine observation, we obtained the data from only one site. The MLH  
157 and backscattering coefficient were measured by enhanced single-lens ceilometers  
158 (Vaisala, CL51, Finland) deployed by the IAP (Tang et al., 2016). Backscattering  
159 coefficient profiles were calculated by referencing the attenuation strobe laser LiDAR  
160 technique (910 nm), which is cited in Tang et al. (2015).

161

## 162 **2.2 Model description and experimental design**

163 To investigate the respective effects of urbanization and aerosols and further determine  
164 the interaction between urbanization and aerosols, a high-resolution regional model  
165 with satisfactory performance is necessary for sensitivity tests. The model used in this  
166 study is the latest available version of RMAPS-ST, which was developed by the  
167 Institute of Urban Meteorology, China Meteorological Administration. RMAPS-ST is  
168 based on the Weather Research and Forecasting (WRF v3.8.1) model (Skamarock et  
169 al., 2008) and its data assimilation system (WRFDA v3.8). The simulation domain was  
170 centered at 37.0 °N, 105.0 °E and implemented with two nested grids with resolutions of

171 9 and 3 km for two domains (D1 and D2, respectively) (Fig 1a). The model performance  
172 was verified, and RMAPS-ST was run operationally (Fan et al., 2018). The assimilation  
173 began every three hours, and the assimilated data included automatic meteorological  
174 station data, sounding data and radar data when available. The model settings are shown  
175 in Table 1. The simulation started at 0000 LST and ran from the 15<sup>th</sup> to 23<sup>rd</sup> of  
176 December 2016 with hourly outputs.

177

178 The urban impact was represented by a high-resolution (30 m) land use map interpreted  
179 from Landsat Thematic Mapper satellite data from 2015 in Beijing. The urban canopy  
180 parameters were optimized according to Miao and Chen (2014). The impact of aerosols  
181 was represented by adding the hourly distribution of AOD in the Rapid Radiation  
182 Transfer Model for General Circulation Models (RRTMG) radiation scheme. The AOD  
183 was extracted from the output of RMAPS-Chem (Zhao et al., 2019; Zhang et al., 2018)  
184 for the BTH region, which is shown in Fig 1b. Anthropogenic emission data were  
185 obtained according to the Multiresolution Emission Inventory for China (2012)  
186 (<http://www.meicmodel.org/>) with a resolution of  $0.1^{\circ} \times 0.1^{\circ}$ . The particle size  
187 distribution and typology of aerosols used in this study is according to Ruiz et al. (2014).  
188 The simulated distribution of AOD in Beijing was verified to be satisfactory after  
189 comparison with the observed vertical profile of the backscattering coefficient (Fig 2a  
190 and b). The correlation between the AOD and the column backscatter coefficient is 0.76  
191 (Fig 2c). Four tests were designed to investigate the impacts of aerosols and  
192 urbanization on typical haze events. Test 1: Both urban and aerosol impacts were  
193 considered in the simulation. We updated the grid AOD distribution hourly as the input  
194 field for the RRTMG radiation scheme in Domain 2. Test 2: Only aerosol impact was  
195 considered in the simulation, and we replaced the urban grids with cropland to shield  
196 the impact of urbanization. Test 3: Only urban impact was considered, and the direct  
197 radiative forcing of aerosols was not considered in the simulation. Test 4: Both urban  
198 and aerosol impacts were not considered in the simulation.

199

200 The model evaluation results for the four tests are shown in Table 2. As the service  
201 operational system, the RMAPS-ST model assessment report indicated that the model  
202 performance was satisfactory (Fan et al. 2018). We evaluated not only the conventional  
203 meteorological variables (including temperature, humidity and wind speed) but also  
204 unconventional but important variables for this study (including radiation and surface  
205 heat flux). A total of 309 meteorological station data points were used to evaluate the  
206 conventional variables. The unconventional variables were evaluated according to the  
207 observational data from 140 m of the Beijing meteorological tower. Test 1 was found  
208 to be the best simulation and considered both the urban and aerosol impacts. The  
209 deficiency of observation sites, interpolation methods and the height differences  
210 between the observations and simulations resulted in higher root mean square error  
211 (RMSE) values for radiation and heat flux than for the other variables.

212

### 213 **3 Results**

#### 214 **3.1 Observation and weather condition analysis**

215 A typical continuous severe heavy haze event occurred from the 15<sup>th</sup> to 22<sup>nd</sup> of  
216 December 2016 in the BTH region. Three stages dominated by three different synoptic  
217 patterns controlled the formation of this haze. In the first stage, northwest airflow in  
218 front of a ridge of high pressure was observed in the BTH region at a height of 700 to  
219 500 hPa and in eastern China at a height of 850 hPa on the 15<sup>th</sup> to 16<sup>th</sup> of December,  
220 which induced a sharp warming pattern (Fig 3a and b). At the surface, Beijing was  
221 located under the front of the high-pressure system to under the southwest airflow in  
222 front of the low-pressure system (Fig 4), which favored pollutant transport from Hebei  
223 Province to Beijing. From the 17<sup>th</sup> to the night of the 18<sup>th</sup>, the control system turned to  
224 latitude circulation at 700 to 500 hPa over the BTH region (there was a trough line south  
225 of 40°N at 2000 LST on the 17<sup>th</sup> and 18<sup>th</sup>) (Fig 3c). There was a northwest wind located  
226 north of 40°N and a southwest wind located south of 40°N at 850 hPa (Fig 3d). The  
227 near surface was controlled by the northeast airflow located in the inverted low-pressure  
228 trough. The weak convergence of the high trough cooperates with the low pressure at



229 the surface, leading to continuous pollution accumulation near the surface. Under this  
230 weather situation, the near-surface temperature began to continuously increase from the  
231 16<sup>th</sup> to 18<sup>th</sup>, and the specific humidity also correspondingly increased (Fig 5a). The near-  
232 surface wind speed and pressure decreased during this period (Fig 5b). The  
233 concentration of PM<sub>2.5</sub> gradually increased from the 16<sup>th</sup>, and the average concentration  
234 of PM<sub>2.5</sub> reached 200  $\mu\text{g}\cdot\text{m}^{-3}$  on the 18<sup>th</sup>. The density of ozone obviously decreased  
235 from the 16<sup>th</sup> (Fig 5c).

236

237 The MLH significantly declined beginning on the 16<sup>th</sup>, and the diurnal cycle almost  
238 disappeared during this period, which was accompanied by a reduction in visibility with  
239 a diurnal variation (Fig 5d). The downward shortwave radiation and the net radiation  
240 gradually decreased from the 16<sup>th</sup> to the 18<sup>th</sup>, which directly influenced the trend of the  
241 variation in ozone (the maximum density of ozone was less than 110  $\text{mg}\cdot\text{m}^{-3}$ ), while  
242 there was little change detected in longwave radiation (Fig 5e). The observed sensible  
243 heat flux also decreased from the 16<sup>th</sup> to the 19<sup>th</sup>, although the temperature increased,  
244 which means that the heat exchange became weaker in the vertical direction, while the  
245 latent heat flux changed little (Fig 5f). Southwest airflow was again captured by a wind  
246 profiler on the night of the 18<sup>th</sup>, and the transport layer occurred from 300 to 1500 m,  
247 which differs from the previous surface transport pattern (Fig 4).

248

249 In the second stage, an important change occurred on the morning of the 19<sup>th</sup> of  
250 December, when the control system turned to the northwest airflow on the front of the  
251 trough over the BTH region at 500 to 850 hPa (Fig 3e and f). After 2000 LST on the  
252 19<sup>th</sup>, obvious warming occurred again at 850 hPa in eastern China (Fig 3h). However,  
253 the near-surface maximum temperature and diurnal range in Beijing significantly  
254 decreased but with high specific humidity during the 20<sup>th</sup> to 21<sup>st</sup> (Fig 5a). According to  
255 the surface weather map, the control system turned to the southwest at 1400 LST on the  
256 19<sup>th</sup>, and a large-scale southeast wind appeared in eastern Beijing after 2000 LST, which  
257 induced wide advection fog formation overnight (Fig 3g). Due to the influence of the

258 southwest airflow on the trough at 500 hPa, the inverted trough moved east, and Beijing  
259 was located in the southeast wind zone. The near-surface pressure increased slightly,  
260 and the wind speed remained low at approximately  $1 \text{ m}\cdot\text{s}^{-1}$  (Fig 5b). The synoptic  
261 system caused the  $\text{PM}_{2.5}$  concentration to peak (approximately  $400 \mu\text{g}\cdot\text{m}^{-3}$  on average  
262 and above  $500 \mu\text{g}\cdot\text{m}^{-3}$  observed at some stations) and was maintained from the 20<sup>th</sup> to  
263 the 21<sup>st</sup> in the BTH region. The visibility was less than 400 m, and the diurnal cycle  
264 disappeared (Fig 5d). The decrease in the downward shortwave and net radiation during  
265 this period was more pronounced than that in the previous three days (Fig 5e). The  
266 sensible heat flux also decreased, and the diurnal cycle almost disappeared from the  
267 19<sup>th</sup> to the 20<sup>th</sup> (Fig 5e). It was not until the strong cold air moved southward in the  
268 early morning of the 22<sup>nd</sup> when the whole atmosphere converted to the northwest stream.  
269 The air pollutants were completely removed in the third stage.

270

271

## 272 **3.2 Interaction between the impacts of urbanization and aerosols on haze events**

273 Four impacts were analyzed as follows. Urban impact under the aero scenario (UI\_aero)  
274 was represented by the results of Test 1 minus those of Test 2; urban impact under the  
275 no-aero scenario (UI\_noaero) was represented by the results of Test 3 minus those of  
276 Test 4; the impact of the urbanization scenario was represented by the results of Test 1  
277 minus those of Test 3 (AI\_urban); the impact without urbanization was represented by  
278 the results of Test 2 minus those of Test 4 (AI\_nourban). The interaction between  
279 urbanization and aerosols on local meteorological and regional transportation was  
280 discussed.

281

### 282 **3.2.1 The impact on the local area**

283 The quantitative results of the interaction between urbanization and aerosols are shown  
284 in Table 3. Temperature is one of the most sensitive variables affected by urbanization  
285 and aerosols and is also the most concerning variable. The impact of urbanization on  
286 the near-surface temperature displays diurnal variation in the Beijing area. The warming

287 effect of urbanization was dominant at night. The urban impact on temperature was  
288 partly offset under aerosol conditions when comparing the results of UI\_aero and  
289 UI\_noaero, especially during the daytime (Fig 6a, red lines). The urban impact always  
290 showed a positive contribution to the temperature throughout the day under the no-  
291 aerosol scenario, while the urban impact became slightly negative during the daytime  
292 under the aerosol scenario. The maximum difference between UI\_aero and UI\_noaero  
293 occurred on the 20<sup>th</sup> and 21<sup>st</sup>, when the AOD value reached its maximum, and the  
294 difference almost disappeared on the 15<sup>th</sup> and 22<sup>nd</sup>, with a small AOD (Fig 2b). The  
295 results indicate that the impact of urbanization on temperature is reduced by aerosols,  
296 which is consistent with the findings of Yang et al. (2020). The average urban impact  
297 on temperature in Beijing during the 16<sup>th</sup> to 19<sup>th</sup> with a PM<sub>2.5</sub> concentration of  
298 approximately 200 mg·m<sup>-3</sup> was a reduction of 0.42°C according to UI\_aero and a  
299 reduction of 0.60°C according to UI\_noaero. This result means that aerosols reduce the  
300 urban impact on temperature by 30%. When the concentration of PM<sub>2.5</sub> reached 500  
301 mg·m<sup>-3</sup> from the 20<sup>th</sup> to the 21<sup>st</sup>, the aerosols reduced urbanization-related warming by  
302 54%.

303

304 The impact of aerosols on temperature is negative and without a diurnal cycle under the  
305 urbanization scenario for the whole day (Fig 6a, blue lines). However, the impact of  
306 aerosols captured by AI\_nourban is significant and displays a diurnal cycle. Another  
307 important observation is that the impact of aerosols on temperature under the no-urban  
308 scenario is not always negative. There is a slight warming period at dawn in the  
309 AI\_nourban scenario, which may be because the longwave radiation is increased  
310 (Jacobson, 1998; Rudich et al., 2007). The average impact of aerosols on temperature  
311 in Beijing was -0.16°C with urbanization and -0.34°C without urbanization from the  
312 16<sup>th</sup> to the 19<sup>th</sup>. The impact of aerosols was -0.19°C with urbanization and -0.43°C  
313 without urbanization from the 20<sup>th</sup> to the 21<sup>st</sup>. Urbanization decreased the impact of  
314 aerosols by 53% under moderate pollution and by up to 56% under heavy pollution.  
315 Two different impacts of aerosols on urban-related warming were observed. There was

316 a reducing effect in the daytime with a strength of approximately 30 to 50% of the  
317 concentration, and an increasing effect occurred at dawn with a strength of  
318 approximately 28%. Urbanization reduced the aerosol-related cooling effect by  
319 approximately 54%.

320

321 The observed specific humidity continued to increase as the aerosol concentration  
322 increased (Fig 5b) and was closely related to the UHI effect and aerosol composition  
323 (Zhang et al. 2010; Sun et al., 2013; Wang et al., 2020). The specific humidity also  
324 increased with urbanization throughout the day (Fig 6b, red lines). Similar to  
325 temperature, urbanization had a more pronounced impact on specific humidity at night.  
326 The average urban impact on specific humidity was  $3.66 \times 10^{-2} \text{ g} \cdot \text{kg}^{-1}$  according to  
327 UI\_aero and  $4.78 \times 10^{-2} \text{ g} \cdot \text{kg}^{-1}$  according to UI\_noaero from the 16<sup>th</sup> to 19<sup>th</sup> and  $3.08 \times 10^{-2}$   
328  $^2$  and  $4.48 \times 10^{-2} \text{ g} \cdot \text{kg}^{-1}$  from the 20<sup>th</sup> to 21<sup>st</sup>. Aerosols not only reduced the urban impact  
329 on the average daily specific humidity by 23.43% but also reduced the diurnal range of  
330 specific humidity.

331

332 In contrast to urbanization, aerosols were found to reduce the specific humidity (Fig 6b,  
333 blue lines). The impact of aerosols under the urbanization scenario was small and did  
334 not exhibit a diurnal pattern. However, the impact of aerosols under the no-urban  
335 scenario was more distinct and exhibited a diurnal cycle. The average impact of aerosols  
336 on specific humidity was  $-0.88 \text{ g} \cdot \text{kg}^{-1}$  according to AI\_urban and  $-1.36 \text{ g} \cdot \text{kg}^{-1}$  according  
337 to AI\_nourban throughout the study period. Urbanization reduced the impact of  
338 aerosols on specific humidity by 35.3%. The impacts of urbanization and aerosols on  
339 humidity were slightly greater than those of aerosols on urban impacts.

340

341 There was no effect of urbanization on downward shortwave radiation according to  
342 both UI\_aero and UI\_noaero (Fig 6c, red lines), although the value was not absolutely  
343 related to aerosols because of model uncertainty. Aerosols reduce the downward  
344 shortwave radiation during the daytime, and the differences between AI\_urban and

345 AI\_nourban are very small.

346

347 The average decrease in shortwave radiation caused by aerosols was approximately 7%  
348 of the total downward shortwave radiation during the 16<sup>th</sup> to the 20<sup>th</sup> and up to 17%  
349 when the PM<sub>2.5</sub> was greater than 400  $\mu\text{g}\cdot\text{m}^{-3}$ . The urban impact increased the longwave  
350 radiation at night according to UI\_aero, while the impact of urbanization was always  
351 positive for longwave radiation during the study period according to UI\_noaero (Fig  
352 6d, red lines). Because it is closely related to temperature, the urban impact on  
353 longwave radiation was also reduced by aerosols, with reductions of 83% from the 16<sup>th</sup>  
354 to the 19<sup>th</sup> and 97% from the 20<sup>th</sup> to the 21<sup>st</sup>. The impact of aerosols on longwave  
355 radiation was less than that of shortwave radiation, and there was a slight decrease  
356 captured by AI\_urban with an increase from noon on the 20<sup>th</sup> to nighttime on the 21<sup>st</sup>.  
357 The impact of aerosols decreased the longwave radiation captured by AI\_nourban  
358 during the 16<sup>th</sup> to the 20<sup>th</sup> and increased it on the night of 21<sup>st</sup> (Fig 6d, blue lines).  
359 Urbanization reduced the impact of aerosols on longwave radiation by 67%, while  
360 aerosols reduced the urban impact on longwave radiation by 89%. The impacts of  
361 urbanization and aerosols on longwave radiation are unimportant because they are both  
362 smaller than  $2\text{ W}\cdot\text{m}^{-2}$ .

363

364 The change in radiation further alters the MLH. Previous studies suggested that the  
365 MLH is important for the diffusion of pollutants and haze formation (Sun et al. 2013;  
366 Quan et al. 2014). Previous studies on urbanization indicated that urban-induced  
367 warming will increase the MLH during the daytime (Wang et al., 2007; Miao et al.  
368 2012), and the results of UI\_noaero showed the same pattern. However, when we  
369 introduced aerosols into the simulation, urbanization was found to decrease the MLH  
370 during the daytime according to UI\_aero. The impact of aerosols decreased the average  
371 urbanization by 148% during the haze event (Fig 6e, red lines). Aerosols significantly  
372 decreased the MLH during the daytime according to both AI\_urban and AI\_nourban  
373 (Fig 6e, blue lines). Urbanization decreased the impact of aerosols on the MLH by 58%

374 during the haze event.

375

376 Urban land use change directly alters the surface heat flux. Urbanization increased the  
377 sensible heat flux according to UI\_noaero but decreased the sensible heat flux  
378 according to UI\_aero (Fig 6f, red lines). The impact of aerosols in reducing the urban  
379 impact on sensible heat flux was 156% during the haze event. Aerosols reduced the  
380 sensible heat flux according to both AI\_urban and AI\_nourban (Fig 6f, blue lines). The  
381 maximum impact of aerosols occurred on the 21<sup>st</sup>, with the maximum AOD. The impact  
382 of urbanization reduced the impact of aerosols on sensible heat flux by 59%.

383

384 There was little effect of urbanization on latent heat flux because the observed latent  
385 heat flux in urban areas was small (Fig 6g, red lines, and Fig 5e). Aerosols decreased  
386 the latent heat flux, and the impact increased with increasing AOD (Fig 6g, blue lines).  
387 The impact of urbanization reduced the impact of aerosols on the latent heat flux by  
388 48%.

389

390 The above results indicate that the offsetting effect of aerosols on urbanization is more  
391 important than the impact of urbanization on aerosols on local weather.

392

### 393 **3.2.2 Effects on regional circulation**

394 There are few valuable findings from the diurnal average wind speed analysis because  
395 the average wind speed was low during the haze event. Wind speed is likely to become  
396 more meaningful during the spatial analysis of wind vectors. There are two main  
397 transmission processes of pollution from Hebei Province to Beijing during this haze  
398 process according to the weather map and wind profile analysis (Fig 4). Accordingly,  
399 the diurnal pattern of PM<sub>2.5</sub> in Beijing (Fig 5c) also displays two increasing processes  
400 on the 16<sup>th</sup> and 19<sup>th</sup> (from 1800 to 2400 LST). The observed near-surface wind vector  
401 displays these two pollutant transport processes (Fig 7). In the first processes, obvious  
402 aerosol transport began on the night of the 15<sup>th</sup> and continued to the night of the 16<sup>th</sup>

403 (Fig 6). The southwest wind dominated most of the southern part of Hebei Province.  
404 The transmission flux was strong during the daytime on the 16<sup>th</sup>, leading to the  
405 concentration of PM<sub>2.5</sub> continuing to increase in Beijing and in its transmission path.  
406 The wind speed remained low from the 17<sup>th</sup> to the 18<sup>th</sup> in most of the plain area, and the  
407 concentration of PM<sub>2.5</sub> continued to increase in the southwest and northeast of Hebei  
408 Province. The second processes began at 1400 LST on the 19<sup>th</sup>, and the south wind  
409 dominated the south of Beijing and turned to the southwest in Beijing at 1400 to 1800  
410 LST. The dominant wind direction turned to the southwest at 2200 LST in the southern  
411 part of Hebei Province with a rapid increase in the concentration of PM<sub>2.5</sub>.

412

413 Most industrial aerosols in Beijing are transported from the southwest and northeast of  
414 Hebei Province due to the control of pollutant discharge in the Beijing area during haze  
415 events. Therefore, the impact of urban areas and aerosols on transport, namely, wind  
416 fields, is very important for air quality in Beijing. The modeling results show that  
417 urbanization not only increased the temperature in urban areas (Fig 8a and b) but also  
418 increased the average south-wind transport flux in the two main transmission processes  
419 of pollution in the southwest area of Beijing (Fig 8a and b). The transmission flux  
420 captured by UI\_noaero was stronger than that captured by UI\_aero. The local cyclonic  
421 circulation induced by urbanization further induced upward movement, which was  
422 beneficial to diffusion conditions. Although aerosols decrease the transmission flux  
423 induced by urbanization, the strength of local cyclonic circulation is also reduced by  
424 aerosols. Furthermore, the aerosols reduced the temperature in most of the plain area in  
425 Hebei Province (Fig 8c and d). Urbanization decreased the impact of aerosols on  
426 temperature. There was no local or systemic effect on the wind field captured by either  
427 AI\_urban or AI\_nourban.

428

429 Taylor diagrams were used to analyze the relative contributions of urbanization and  
430 aerosols over time (Fig 9). The daily mean differences in these four types of impact  
431 (UI\_aero, UI\_noaero, AI\_urban, and AI\_nourban) over the eight days in the Beijing

432 area are shown by Taylor diagrams. UI\_noaero shows that temperature continued to  
433 increase from Day 1 to Day 5 and reached a maximum on Day 7. The variation in  
434 temperature according to UI\_aero was small. This result means that the effect of  
435 urbanization on temperature is decreased by aerosols. Temperature increased from Day  
436 1 to Day 7 according to AI\_urban, while AI\_nourban showed an increase from Day 3  
437 to Day 7. The reduction in the urban impact on temperature by aerosols was more  
438 important than the reduction in aerosol impact on temperature by urbanization (Fig 9a).  
439 The effect of aerosols on the urban impacts on temperature was more important than  
440 the urban impacts on the effects of aerosols on temperature (Fig 9a).

441

442 Specific humidity continued to increase from Day 1 to Day 5 according to UI\_noaero,  
443 while the variation in specific humidity was small according to UI\_aero (Fig 9b).  
444 Similar to what was observed for temperature, reducing the urban impact on specific  
445 humidity by aerosols is more important than reducing the impacts to aerosols by urban  
446 areas. The ventilation coefficient (VC) in UI\_aero showed little change over these eight  
447 days, and this coefficient showed increases on Days 2, 3, 5, and 6 and decreases on  
448 Days 4, 7, and 8 according to UI\_noaero. The reduction in the urban impact on the VC  
449 by aerosols was more important than the reduction in the impact of aerosols by  
450 urbanization. The analysis of shortwave radiation also provided the same conclusion  
451 that the reduction in the urban impact on the daily mean by aerosols was more important  
452 than the reduction in the impact of aerosols by urbanization (Fig 9d).

453

### 454 **3.2.3 Impacts on the vertical distribution**

455 In the period from 0000 LST to 0800 LST on the 16<sup>th</sup> to 20<sup>th</sup>, there was an interesting  
456 phenomenon that temperature was slightly larger in UI\_aero than in UI\_noaero, and the  
457 urban impact reached a maximum at the same time. Such an outcome is easy to overlook  
458 if the analysis focuses on only the daily average. Therefore, a detailed vertical  
459 temperature and wind field analysis of the four addressed scenarios (UI\_aero,  
460 UI\_noaero, AI\_urban, and AI\_nourban) was used to determine the mechanism behind



461 this finding (Fig 10).

462

463 The impact on warming by urbanization reached 350 m in UI\_aero and 450 m in  
464 UI\_noaero (Fig 10a and b). Aerosols not only increased the warming impact induced  
465 by urbanization but also reduced the warming height. Aerosols increase the near-surface  
466 warming effect induced by urbanization because of the absorption of longwave  
467 radiation. Although absorption by aerosols was always observed during the study period,  
468 the impact increased with the increase in longwave radiation induced by urbanization.  
469 Therefore, the warming effect of aerosols may dominate at night in the near-surface  
470 layer. This effect further induces urban-related warming to increase and compress this  
471 effect to a lower height with a lower MLH in UI\_aero than in UI\_noaero (Fig 10a). The  
472 aerosols reduced the temperature below 450 m in the urban area of Beijing (Fig 10c and  
473 d), and the cooling effect was reduced by urbanization below 450 m. Urbanization also  
474 reduced the near-surface west wind induced by aerosols in urban areas because of the  
475 drag caused by buildings.

476

#### 477 **4 Conclusion**

478 A typical persistent haze process occurred on the 15<sup>th</sup> to 22<sup>nd</sup> of December 2016 in the  
479 BTH region. The average concentration of PM<sub>2.5</sub> was approximately 200  $\mu\text{g}\cdot\text{m}^{-3}$ , and  
480 the maximum was 695  $\mu\text{g}\cdot\text{m}^{-3}$ . The interaction between aerosols and urbanization on  
481 haze events was investigated in this study. Four tests were designed using RMAPS-ST  
482 to study the mechanism of the impacts of aerosols and urbanization.

483

484 Two different impacts of aerosols on urban-related warming were found. A reducing  
485 effect occurred during the daytime, and the strength was approximately 30 to 50% of  
486 the concentration. An increasing effect occurred at dawn, and the strength was  
487 approximately 28%, which is important for haze formation. The combined effect was a  
488 reducing effect on the daily mean of urban-related warming. Urbanization reduced the  
489 aerosol-related cooling effect by approximately 54% during the haze event, and the

490 strength of the impact changed little with increasing aerosol content. The impact of  
491 urbanization on the effect of aerosols on humidity is slightly larger than the impact of  
492 aerosols on urban impact. Aerosols reduce the average downward shortwave radiation  
493 from 7% to 17% with concentrations of PM<sub>2.5</sub> of 200 to 400  $\mu\text{g}\cdot\text{m}^{-3}$ . There is no urban  
494 impact on downward shortwave radiation or an impact of aerosols on shortwave  
495 radiation. The impacts of urban areas and aerosols on longwave radiation are both  
496 smaller than  $2\text{ W}\cdot\text{m}^{-2}$ . The most significant impact of aerosols is observed on the MLH  
497 and sensible heat flux. The decrease in urban impact caused by aerosols reaches 148%  
498 for MLH and 156% for sensible heat flux. These values are much larger than those for  
499 urbanization, which reduces the impact of aerosols on the MLH and sensible heat flux.  
500 There is little urban impact on latent heat flux. However, aerosols decreased the latent  
501 heat flux, and the impact was reduced by 48.8% by urbanization. In general, the impact  
502 of aerosols on urban impact is more important than the impact of urbanization on  
503 aerosol impacts in terms of regional averages.

504

505 Urbanization increased the wind speed southwest of the Beijing area and the local  
506 cyclonic circulation in the urban area of Beijing during the two main transmission  
507 processes. Although aerosols reduced the urban-related southwest transmission, they  
508 worsened the diffusion conditions in urban areas. The impact of urbanization on wind  
509 fields, namely, the transport of pollutants, is more important than that of aerosols.  
510 However, the interaction between urbanization and aerosols may enhance the  
511 accumulation of pollution and weigh against diffusion.

512

513 The impact of aerosols on urban-related warming is more significant than the impact of  
514 urbanization on aerosol-related cooling according to spatial statistical analysis. Similar  
515 results were found for absolute humidity, VC and shortwave radiation. Aerosol-related  
516 warming is dominant at dawn in the near-surface layer. Aerosols increase urban-related  
517 warming and reduce the impact height of urban-related warming. This further enhances  
518 stability and reduces the MLH.

519 **5 Discussion**

520 In this study, it was easier to distinguish the impacts of aerosols and urbanization by  
521 using RMAPS-ST with AOD hourly inputs than with RMAPS-Chem. One reason for  
522 this difference is that the model performance of RMAPS-ST is much better than that of  
523 RMAPS-Chem in meteorological fields. Although real-time feedback in modeling is  
524 not provided, RMAPS-ST is more efficient and more suitable for short-term operational  
525 forecasting.

526

527 This study not only qualified the impacts of aerosols and urbanization on haze events  
528 but also analyzed the interaction between aerosols and urbanization during haze events.  
529 This research will help to improve air quality under the continuous  
530 urbanization and sustainable development of large cities.

531

532 The government has taken a series of emission reduction measures, including limiting  
533 industrial emissions and vehicle plate number traffic restriction measures, to improve  
534 the air quality in the BTH region. The policies have been effective in reducing aerosols.  
535 At the same time, urbanization continues mainly in the areas around Beijing (such as  
536 the Xiongan New Area). The results of this study show that the combined impact of  
537 urbanization and decreasing aerosols will increase the downward shortwave radiation  
538 and further increase the surface temperature and ozone concentration in the boundary  
539 layer. Previous studies indicated that ozone generally increases with temperature and  
540 decreases with humidity (Camalier et al., 2007; Cardelino et al., 1990). It is well known  
541 that ozone is not only a pollutant but also a greenhouse gas. Therefore, ozone will form  
542 a positive feedback mechanism to induce warming and ozone pollution in the boundary  
543 layer. This feedback will pose a new challenge regarding how to reduce ozone pollution  
544 in urban areas. Some studies have suggested that urban greening can effectively reduce  
545 ozone pollution (Nowak et al., 2000; Benjamin and Winer, 1998). More attempts should  
546 be made to add the interaction between urbanization and ozone in regional models.

547

548 **Acknowledgments**

549 This work was supported by the Beijing National Science Foundation of China  
550 (Grant No. 8171002), the National Natural Science Foundation (41705088) and  
551 the National Key R&D Program of China (2019YFA0607202).

552

553 **Data availability**

554 The data in this study are available from the corresponding author upon request  
555 ([tgq@dq.cern.ac.cn](mailto:tgq@dq.cern.ac.cn)).

556

557 **Author contribution**

558 Miao Yu designed the research and wrote the paper. Guiqian Tang conducted the  
559 measurements and reviewed the paper. Yang Yang conducted modeling tests. Qingchun  
560 Li and Yonghong Wang performed synoptic analysis. Shiguang Miao, Yizhou Zhang  
561 and Yusi Wang reviewed and commented on the paper.

562

563 **Competing interests**

564 The authors declare that they have no conflicts of interest to disclose.

565

566 Table 1 RMAPS-ST model settings.

| WRF v3.8.1                   | D01  | D02     |
|------------------------------|--|---------|
| Horizontal grid              | 649×400                                    | 550×424 |
| Grid horizontal spacing (km) | 9  | 3       |
| Vertical layers              | 49   |         |
| PBL                          | YSU (Hong et al., 2006)                    |         |
| Microphysics                 | Thompson (Thompson et al., 2008)           |         |
| Cumulus                      | Kain-Fritsch (Kain, 2004)                  | None    |
| LW radiation                 | RRTMG                                      |         |
| SW radiation                 | RRTMG                                      |         |
| LSM                          | Noah LSM+SLUCM                             |         |
| Urban parameter values       | Modified according to Miao and Chen (2014) |         |

567

568  
569  
570  
571  
572

Table 2 Model evaluation (RMSE and BIAS) for the four tests.

|               | Test 1       |              | Test 2 |       | Test 3 |       | Test 4 |       |
|---------------|--------------|--------------|--------|-------|--------|-------|--------|-------|
|               | RMSE         | BIAS         | RMSE   | BIAS  | RMSE   | BIAS  | RMSE   | BIAS  |
| Temperature   | <b>1.27</b>  | <b>0.35</b>  | 1.45   | -0.73 | 2.12   | 1.04  | 1.78   | -0.45 |
| Specific      | <b>0.26</b>  | -            | 0.31   | 0.019 | 0.34   | -0.05 | 0.29   | 0.03  |
| Wind speed    | <b>1.62</b>  | <b>0.97</b>  | 2.08   | 1.68  | 1.85   | 1.04  | 1.96   | 1.67  |
| Shortwave     | <b>40.91</b> | <b>11.85</b> | 40.95  | 11.89 | 47.35  | 17.45 | 46.26  | 16.45 |
| Longwave      | <b>51.39</b> | -            | 51.32  | -     | 51.24  | -     | 52.76  | 44.97 |
| Sensible heat | <b>8.09</b>  | <b>-1.19</b> | 9.13   | -3.92 | 9.34   | -3.43 | 12.3   | -6.17 |
| Latent heat   | <b>14.09</b> | <b>-5.75</b> | 14.52  | -5.95 | 14.85  | -5.87 | 16.76  | -6.23 |

573  
574  
575  
576  
577  
578

Table 3 Quantitative results of the interaction between urbanization and aerosols

| Time       | Temperature<br>°C                  |                                    | Specific humidity<br>×10 <sup>-2</sup> g kg <sup>-1</sup> |                                    | Longwave<br>W·m <sup>-2</sup>      |                                    | MLH<br>m                           | Sensible heat<br>flux W·m <sup>-2</sup> | Latent heat<br>flux W·m <sup>-2</sup> |
|------------|------------------------------------|------------------------------------|---|------------------------------------|------------------------------------|------------------------------------|------------------------------------|---|---------------------------------------|
|            | 16 <sup>th</sup> -19 <sup>th</sup> | 20 <sup>th</sup> -21 <sup>st</sup> | 16 <sup>th</sup> -19 <sup>th</sup>                        | 20 <sup>th</sup> -21 <sup>st</sup> | 16 <sup>th</sup> -19 <sup>th</sup> | 20 <sup>th</sup> -21 <sup>st</sup> | 16 <sup>th</sup> -21 <sup>st</sup> | 16 <sup>th</sup> -21 <sup>st</sup>      | 16 <sup>th</sup> -21 <sup>st</sup>    |
| UI_aero    | 0.42                               | 0.19                               | 3.66  | 3.08                               | 0.10                               | -0.02                              | -1.97                              | -1.01                                   | 0.03                                  |
| UI_noaero  | 0.60                               | 0.35                               | 4.78  | 4.48                               | 0.62                               | 0.51                               | 4.04                               | 1.74                                    | 0.49                                  |
| AI_urban   | -0.16                              | -0.19                              | -0.88   |                                    | -0.24                              |                                    | -4.37                              | -1.64                                   | -0.50                                 |
| AI_nourban | -0.34                              | -0.43                              | 1.36  |                                    | -0.73                              |                                    | -10.38                             | -4.02                                   | -0.96                                 |

579  
580

581 **References**

- 582 Benjamin, M. T., Winer, A. M.: Estimating the ozone-forming potential of urban trees and shrubs,  
583 Atmospheric Environment, 32(1), 53-68, 1998.
- 584 Camalier, L., Cox, W. , and Dolwick, P.: The effects of meteorology on ozone in urban areas and  
585 their use in assessing ozone trends, Atmospheric Environment, 41(33), 7127-7137, 2007.
- 586 Cao, C., Lee, X., Liu, S., Schultz, N., Xiao, W., Zhang, M., and Zhao, L.: Urban heat islands in  
587 China enhanced by haze pollution, Nature Communications, 7(1), 1-7, 2016.
- 588 Cardelino, C. A., and Chameides, W. L.: Natural hydrocarbons, urbanization, and urban  
589 ozone, Journal of Geophysical Research, 95(D9), 13971, 1990.
- 590 Chen, H., and H. Wang: Haze Days in North China and the associated atmospheric circulations  
591 based on daily visibility data from 1960 to 2012, J. Geophys. Res. Atmos., 120, 5895–5909,  
592 2015.
- 593 Coulter, R.L.: A Comparison of three methods for measuring mixing-layer height, J Appl  
594 Meteor,18(11):1495-1499, 1979.
- 595 Crutzen, P. J.: New directions: the growing urban heat and pollution ‘island’ effect-impact on  
596 chemistry and climate, Atmos. Environ, 38, 3539–3540, 2004.
- 597 Fan, S.: Assessment report of regional high resolution model (RMAPS-ST), IUM Technical Note  
598 IUM/2018-1, Beijing, China: IUM, 2018.
- 599 Folberth, G. A., Rumbold, S. T., Collins, W. J., and Butler, T. M.: Global radiative forcing and  
600 megacities, Urban Climate., 1, 4–19, 2014.
- 601 Grimm, N. B. et al.: Global change and the ecology of cities, Science, 319 (5864), 756–760, 2008.
- 602 Grimmond, C.S. B., Kuttler, W., Lindqvist, S., and Roth, M.: Urban climatology icuc6, International  
603 Journal of Climatology, 27(14), 1847-1848, 2010.
- 604 Grimmond, S.U. E.: Urbanization and global environmental change: local effects of urban warming,  
605 Geographical Journal, 173(1), 83-88, 2007.
- 606 Guo, J., Miao, Y., Zhang, Y., Liu, H., Li, Z., Zhang, W., ...and Zhai, P.: The climatology of planetary  
607 boundary layer height in China derived from radiosonde and reanalysis data, Atmospheric  
608 Chemistry and Physics, 16(20), 13309-13319, 2016.
- 609 Huang, J., Minnis, P., Yi, Y., Tang, Q., Wang, X., Hu, Y., ... and Winker, D. M.: Summer dust aerosols  
610 detected from CALIPSO over the Tibetan Plateau, Geophysical Research Letters, 34(18),  
611 DOI:10.1029/2007GL029938, 2007.
- 612 Huang, J., Minnis, P., Chen, B., Huang, Z., Liu, Z., Zhao, Q., ... and Ayers, J. K.: Long-range  
613 transport and vertical structure of Asian dust from CALIPSO and surface measurements during  
614 PACDEX, Journal of Geophysical Research, 113, DOI:10.1029/2008JD010620., 2008a.
- 615 Huang J., W. Zhang, J. Zuo, J. Bi, J. Shi, X. Wang, Z. Chang, Z. Huang, S. Yang, B. Zhang, G. Wang,  
616 G. Feng, J. Yuan, L. Zhang, H. Zuo, S. Wang, C. Fu and J. Chou.: An overview of the semi-arid  
617 climate and environment research observatory over the Loess Plateau, Advances in Atmospheric  
618 Sciences, 25(6), 1-16. DOI: 10.1007/s00376-008-0906-7, 2008b.
- 619 Hong, S. Y., Noh, Y., and Dudhia, J.: A new vertical diffusion package with an explicit treatment of  
620 entrainment processes, Monthly Weather Review, 134, 2318–2341, 2006.
- 621 Jacobson, M. Z.: Studying the effects of aerosols on vertical photolysis rate coefficient and  
622 temperature profiles over an urban airshed, Journal of Geophysical Research, 103,10593–10604,

623 1998.

624 Kain, J. S.: The Kain–Fritsch convective parameterization: An update, *Journal of Applied*  
625 *Meteorology*, 43, 170–181, 2004.

626 Li, D. and Bou-Zeid, E.: Synergistic interaction between urban heat islands and heat waves: the  
627 impact in cities is larger than the sum of its parts, *J. Appl. Meteorol. Climatol*, 52, 2051–2064,  
628 2013.

629 Liu, Q., Geng, H., Chen Y.: Vertical distribution of aerosols during different intense dry haze period  
630 around Shanghai, *China Environmental Science (in Chinese)*, 32(2), 207-213, 2012.

631 Miao, S, Dou J., Chen, F., Li, J., and Li A.: Analysis of observations on the urban surface energy  
632 balance in Beijing, *Science China Earth Sciences*, 055(11), 1881-1890, 2012.

633 Miao, S. and Chen, F.: Enhanced modeling of latent heat flux from urban surfaces in the  
634 Noah/single-layer urban canopy coupled model, *Science China Earth Sciences*, 057(10), 2408-  
635 2416, 2014.

636 Miao, S., Chen, F., Li, Q., and Fan, S.: Impacts of urban processes and urbanization on summer  
637 precipitation: A case study of heavy rainfall in Beijing on 1 August 2006, *Journal of Applied*  
638 *Meteorology and Climatology*, 50, 806–825, <https://doi.org/10.1175/2010JAMC2513.1>, 2011

639 Miao, Y., Guo, J., Liu, S., Liu, H., Li, Z., Zhang, W., and Zhai, P.: Classification of summertime  
640 synoptic patterns in Beijing and their associations with boundary layer structure affecting aerosol  
641 pollution., *Atmos. Chem. Phys*, 17(4), 3097-3110, 2017.

642 Nowak, D. J., Civerolo, K. L., Rao, S. T., Sistla, G., Luley, C. J., and Crane, D. E.: A modeling study  
643 of the impact of urban trees on ozone, *Atmospheric Environment*, 34(10), 1601-1613, 2000.

644 Oke, T.R.: The energetic basis of the urban heat island, *Quarterly Journal of the Royal*  
645 *Meteorological Society*, 108, 1–24, 1982.

646 Oke, T.R.: The heat island of the urban boundary layer: Characteristics, causes and effects, *Wind*  
647 *Climate in Cities*, 81-107, 1995.

648 Pei, L., Yan, Z., Chen, D., & Miao, S.: Climate variability or anthropogenic emissions: which caused  
649 Beijing Haze? *Environmental Research Letters*, 15(3), 034004, 2020.

650 Quan, J., Tie, X., Zhang, Q., Liu, Q., Li, X., and Gao, Y., et al.: Characteristics of heavy aerosol  
651 pollution during the 2012–2013 winter in Beijing, China, *Atmospheric Environment*,  
652 88(Complete), 83-89, 2014.

653 Ren, Y., Zhang, H., Wei, W., Wu, B., Cai, X., and Song, Y.: Effects of turbulence structure and  
654 urbanization on the heavy haze pollution episodes, *Atmospheric Chemistry and Physics*, 19,  
655 1041-1057, 2019.

656 Rudich, Y., Donahue, N. M. & Mentel, T. F. Aging of organic aerosol: bridging the gap between  
657 laboratory and field studies, *Ann. Rev. Phys. Chem.*, 58,321–352, 2007.

658 Ruiz-Arias, J. A., Dudhia, J., & Gueymard, C. A.: A simple parameterization of the short-wave  
659 aerosol optical properties for surface direct and diffuse irradiances assessment in a numerical  
660 weather model. *Geoscientific Model Development*, 7(3), 1159-1174, 2014. Skamarock, W. C.,  
661 Klemp, J. B., Dudhia, J., Gill, D. O., Barker, D., Wang, W., and Powers, J. G.: A description of  
662 the advanced research WRF version 3, NCAR/TN-475 + STR, 2008.

663 Sun, Y., Wang, Z., Fu, P., Jiang, Q., Yang, T., Li, J., and Ge, X.: The impact of relative humidity on  
664 aerosol composition and evolution processes during wintertime in Beijing, China, *Atmospheric*  
665 *Environment*, 77, 927-934, 2013.

666 Taha, H.: Urban climates and heat islands: albedo, evapotranspiration, and anthropogenic heat,  
667 Energy and Buildings, 25, 99–103, 1997.

668 Tang, G., Zhu, X., Hu, B., Xin, J., and Wang, Y.: Impact of emission controls on air quality in Beijing  
669 during APEC 2014: lidar ceilometer observations, Atmospheric Chemistry and Physics, 15(21),  
670 12667-12680, 2015.

671 Tang, G. , Zhang, J. , Zhu, X. , Song, T. , and Wang, Y. : Mixing layer height and its implications  
672 for air pollution over Beijing, China, Atmospheric Chemistry and Physics, 16(4), 2459–2475,  
673 2016.

674 Tao, W., Liu, J., Ban-Weiss, G. A., Hanglustaine, D. A., Zhang, L., Zhang, Q.,... and Tao, S.: Effects  
675 of urban land expansion on the regional meteorology and air quality of eastern China,  
676 Atmospheric Chemistry and Physics, 15(15), 8597–8614, [https://doi.org/10.5194/acp-15-8597-](https://doi.org/10.5194/acp-15-8597-2015)  
677 2015, 2015.

678 Thompson, G., Field, P. R., Rasmussen, R. M., & Hall, W. D.: Explicit forecasts of winter  
679 precipitation using an improved bulk microphysics scheme. Part II: Implementation of a new  
680 snow parameterization, Monthly Weather Review, 136, 5095–5115, 2008.

681 Wang, K., Wang, J., Wang, P., Sparrow, M., Yang, J., Chen, H.: Influences of urbanization on  
682 surface characteristics as derived from the Moderate-Resolution Imaging Spectroradiometer:  
683 A case study for the Beijing metropolitan area, Journal of Geophysical Research, 112 (D22),  
684 doi:10.1029/2006jd007997, 2007.

685 Wang, Y., Yu, M., Wang, Y., Tang, G., Song, T., Zhou, P., ... and Zhu, X.: Rapid formation of intense  
686 haze episodes via aerosol–boundary layer feedback in Beijing, Atmospheric Chemistry and  
687 Physics, 20(1), 45-53, 2020.

688 Wei, W., Zhang, H., Wu, B., Huang, Y., Cai, X., Song, Y., and Li, J.: Intermittent turbulence  
689 contributes to vertical dispersion of PM<sub>2.5</sub> in the North China Plain: cases from Tianjin,  
690 Atmospheric Chemistry and Physics, 18, 12953–12967, [https://doi.org/10.5194/acp-18-12953-](https://doi.org/10.5194/acp-18-12953-2018)  
691 2018, 2018.

692 Wu, D., Wu, X, Li, F., et al.: Temporal and spatial variation of haze during 1951-2005 in Chinese  
693 mainland, Acta Meteorologica Sinica (in Chinese), 68(5), 680-688, 2010.

694 Xu, X., Chen, F., Barlage, M., Gochis, D., Miao, S., and Shen, S.: Lessons learned from modeling  
695 irrigation from field to regional scales, Journal of Advances in Modeling Earth Systems, 11,  
696 2428–2448, <https://doi.org/10.1029/2018MS001595>, 2019.

697 Yang, Y., Zheng, Z., Yim, S. Y. L., Roth, M., Ren, G., Gao, Z., et al.: PM<sub>2.5</sub> pollution modulates  
698 wintertime urban heat island intensity in the Beijing - Tianjin - Hebei Megalopolis, China,  
699 Geophysical Research Letters, 47, e2019GL084288. <https://doi.org/10.1029/2019GL084288>,  
700 2020.

701 Yu, M., and Y. Liu: The possible impact of urbanization on a heavy rainfall event in Beijing,  
702 Journal of Geophysical Research: Atmospheres , 120, 8132–8143, doi:10.1002/2015JD023336,  
703 2015.

704 Yu, M., Miao, S., and Li, Q.: Synoptic analysis and urban signatures of a heavy rainfall on 7 August  
705 2015 in Beijing, Journal of Geophysical Research: Atmospheres, 122, 65–78,  
706 <https://doi.org/10.1002/2016JD025420>, 2017.

707 Yu, M., Y. M. Liu, Y. F. Dai, et al.: Impact of urbanization on boundary layer structure in Beijing,  
708 Climatic Change, 120(1-2), 123-136, 2013.



709 Zhai, S.X, Jacob, Daniel, Wang, X., Lu, S., Li, K., Zhang, Y.Z., Gui, K., Zhao, T.L., and Liao,  
710 H.: Fine particulate matter (PM<sub>2.5</sub>) trends in China, 2013–2018: contributions from meteorology,  
711 Atmospheric Chemistry and Physics, 19(16), 11031-11041, 2019.

712 Zhang, C., Liu, C., Hu, Q., Cai, Z., Su, W., Xia, C., ... and Liu, J.: Satellite UV-Vis spectroscopy:  
713 implications for air quality trends and their driving forces in China during 2005–2017, Light-  
714 Science & Applications, 8(1), 1-12, 2019. Zhang, N., Gao, Z., Wang, X., and Chen, Y.: Modeling  
715 the impact of urbanization on the local and regional climate in Yangtze River Delta,  
716 China, Theoretical and applied climatology, 102(3-4), 331-342, 2010.

717 Zhang, W., Zhuang, G., Guo, J., Xu, D., Wang, W., and Baumgardner, D.,... and Yang, W.: Sources  
718 of aerosol as determined from elemental composition and size distributions in  
719 Beijing, Atmospheric Research, 95(2-3), 0-209, 2010.

720 Zhang, Z., Zhao, X., Xiong, Y., Ma, X.H.: The Fog/Haze Medium-range Forecast Experiments  
721 Based on Dynamic Statistic Method, Journal of Applied Meteorological Science (in Chinese),  
722 29(1),57-69, 2018.

723 Zhao, P., Xu, X., Meng, W. Dong, ... and Zhang, X.L.: Characteristics of haze days in the region of  
724 Beijing, Tianjin, and Hebei, China Environmental Science (in Chinese), 31(1), 31-36, 2012.

725 Zhao, X., Li, Z., and Xu, J.: Beijing regional environmental meteorology prediction system and its  
726 performance test of PM<sub>2.5</sub> concentration, Journal of Applied Meteorological Science (in  
727 Chinese), 27(2),160-172, 2016.

728 Zhao, X.J., Li, Z.M., Xu, J.: Modification and performance tests of visibility parameterizations for  
729 haze days. Environmental. Science, 40 (4), 1688–1696 (in Chinese), 2019.

730 Zhong, S., Qian, Y., Sarangi, C., Zhao, C., Leung, R., Wang, H.,... and Yang, B.: Urbanization effect  
731 on winter haze in the Yangtze River Delta region of China, Geophysical Research Letters, 45,  
732 6710–6718, <https://doi.org/10.1029/2018GL077239>, 2018.

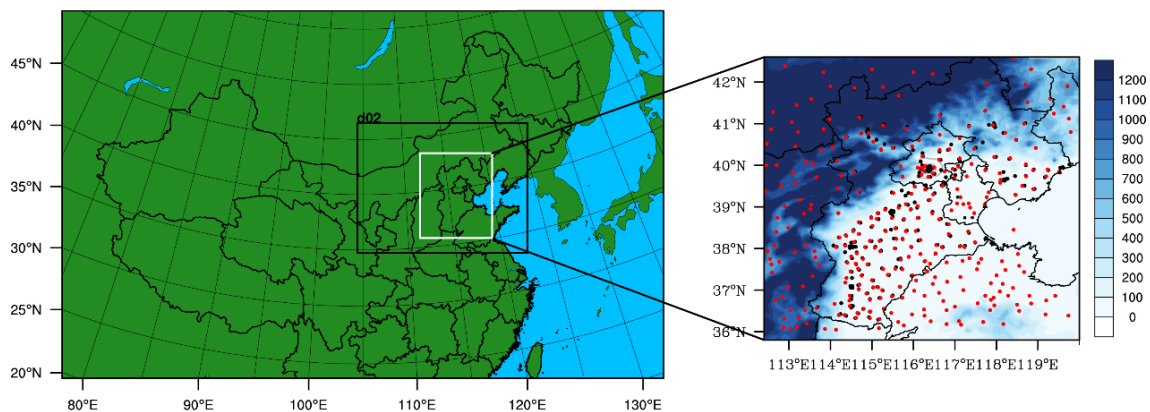
733 Zhong, S., Qian, Y., Zhao, C., Leung, R., and Yang, X. Q.: A case study of urbanization impact on  
734 summer precipitation in the Greater Beijing Metropolitan Area: Urban heat island versus aerosol  
735 effects, Journal of Geophysical Research: Atmospheres, 120, 10,903–10,914.  
736 <https://doi.org/10.1002/2015JD023753>, 2015.

737 Zhong, S., Qian, Y., Zhao, C., Leung, R., Wang, H. L., Yang, B., ... and Liu, D.: Urbanization-  
738 induced urban heat island and aerosol effects on climate extremes in the Yangtze River Delta  
739 region of China. Atmospheric Chemistry and Physics, 17(8), 5439–5457,  
740 <https://doi.org/10.5194/acp-17-5439-2017/>, 2017.

741 Zhu, X., Tang, G., Guo, J., Hu, B., Song, T., Wang, L., Xin, J., Gao, W., Munkel, C., Schäfer, K., Li,  
742 X., and Wang, Y.: Mixing layer height on the North China Plain and meteorological evidence of  
743 serious air pollution in southern Hebei, Atmospheric Chemistry and Physics, 18, 4897–4910,  
744 <https://doi.org/10.5194/acp-18-4897-2018>, 2018.

745  
746  
747  
748  
749  
750  
751

752 **Figure**



753

754 Figure 1 Domain configuration of RMAPS-ST and the location of the study area, indicated by the

755 solid white line. The black dots indicate the locations of the 251 environmental monitoring stations,

756 and the red dots represent the 309 meteorological stations in the BTH region, where the gray loop

757 lines show the locations of the second to sixth ring roads. The shading is the terrain height (unit: m).

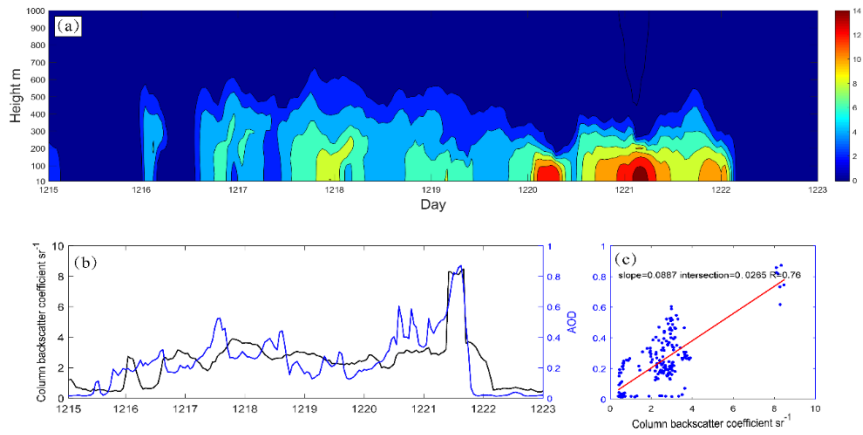
758

759

760

761

762

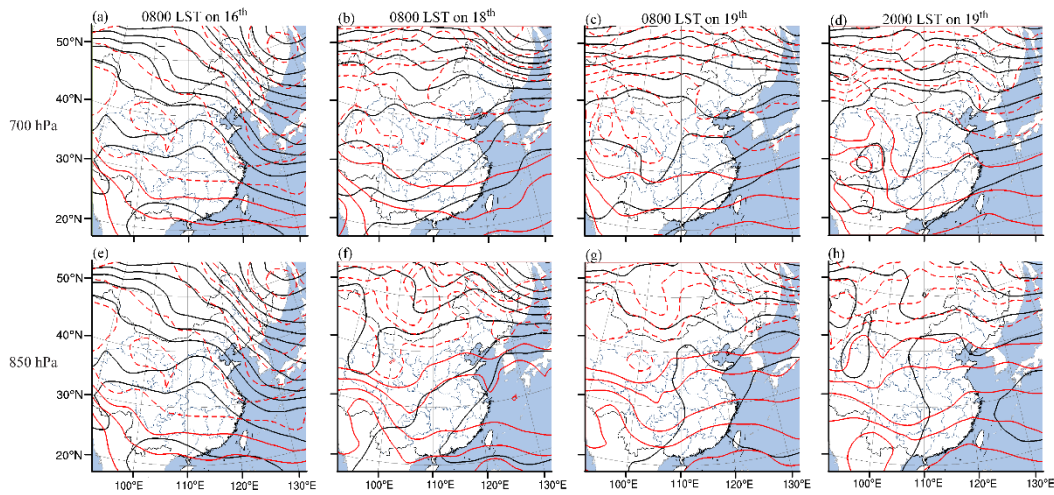


763

764 Figure 2 (a) Hourly backscattering coefficient (shading;  $\text{Mm}\cdot\text{sr}^{-1}$ ) observed by single-lens  
 765 ceilometers ( $39.97^\circ\text{N}$ ,  $116.37^\circ\text{E}$ ) from the 15<sup>th</sup> to 23<sup>rd</sup> of December; (b) hourly column backscatter  
 766 coefficient (black line;  $\text{sr}^{-1}$ ) and AOD used in modeling for Beijing (blue line) and (c) scatter  
 767 diagram of hourly column backscatter coefficient and AOD (blue dots) and their correlations (red  
 768 line).

769

770



771

772 Figure 3 Weather maps. (a) 0800 LST on the 16<sup>th</sup> at 700 hPa; (b) 0800 LST on the 18<sup>th</sup> at 700 hPa;

773

774 (c) 0800 LST on the 19<sup>th</sup> at 700 hPa; (d) 2000 LST on the 19<sup>th</sup> at 700 hPa; (e) 0800 LST on the

775

776 16<sup>th</sup> at 850 hPa; (f) 800 LST on the 18<sup>th</sup> at 850 hPa; (g) 0800 LST on the 19<sup>th</sup> at 850 hPa; (h) 2000

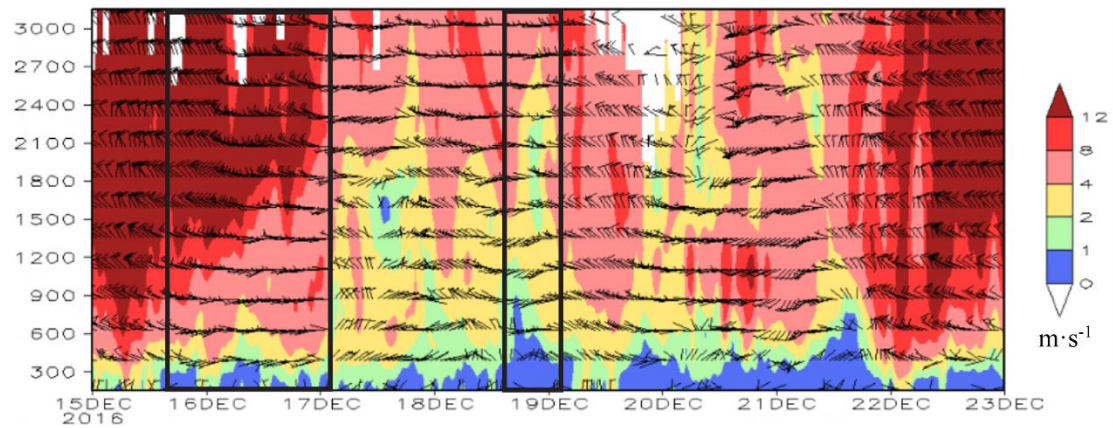
777

778

779

780

781

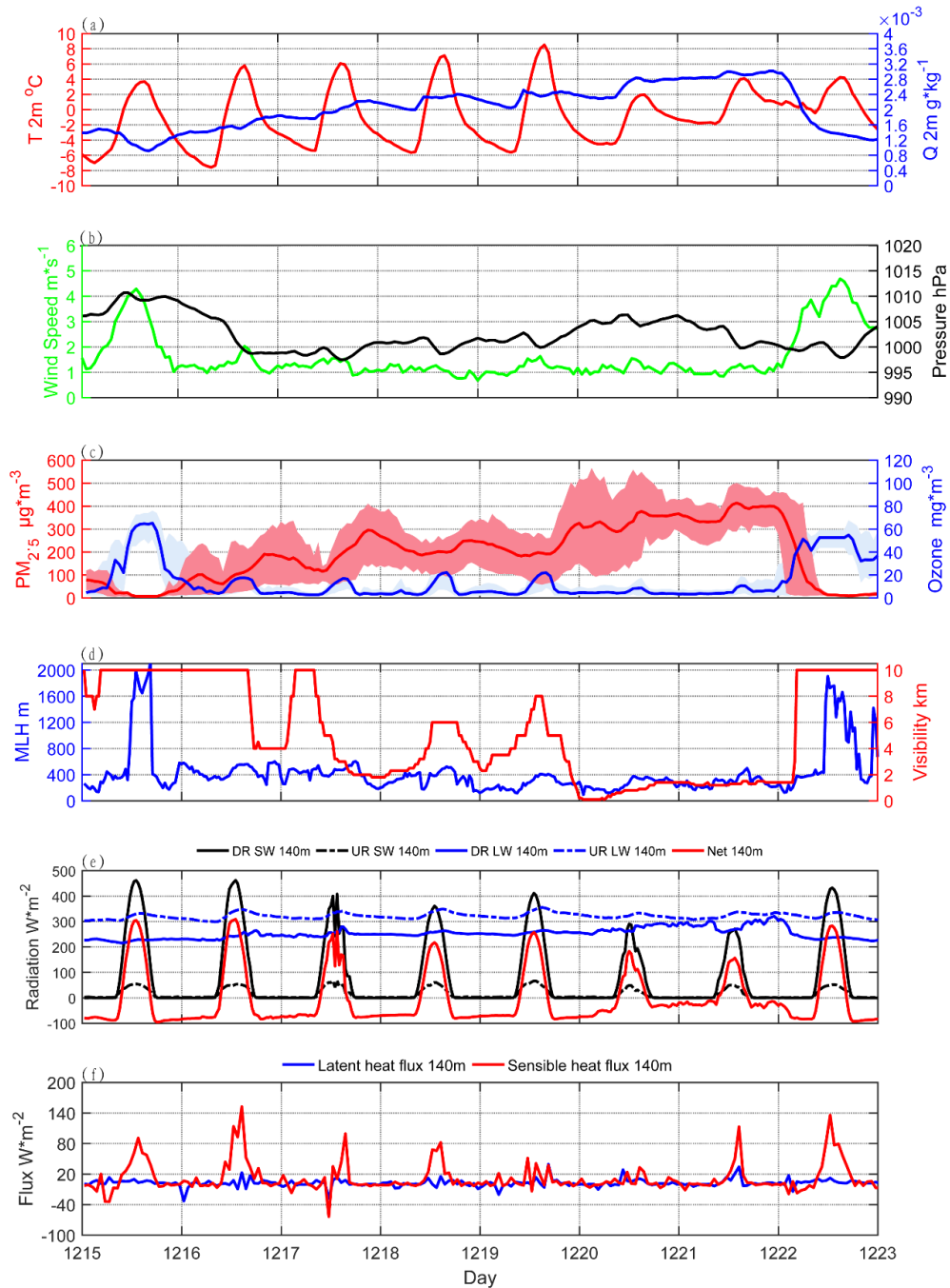


782

783 Figure 4 Hourly wind profile from the 15<sup>th</sup> to 23<sup>rd</sup> of December. Wind speed (shading;  $\text{m}\cdot\text{s}^{-1}$ ) and

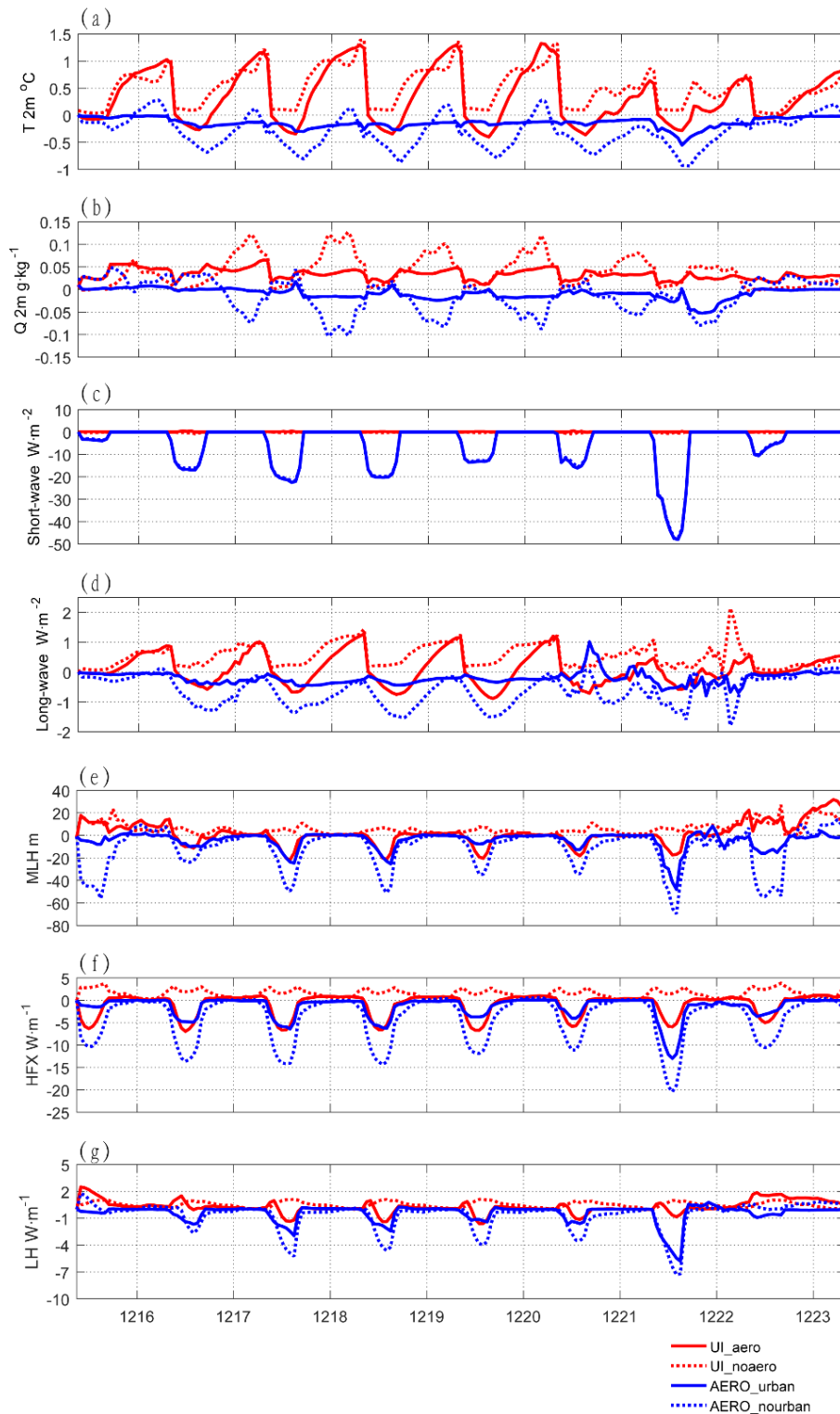
784

785 horizontal wind field (vector;  $\text{m}\cdot\text{s}^{-1}$ ). The black boxes show the two periods of south wind conveyance.



786

787 Figure 5 Diurnal pattern of observed variables from the 15<sup>th</sup> to 23<sup>rd</sup> of December in Beijing. (a)  
 788 Temperature (red line; °C) and absolute humidity (blue line; g kg<sup>-1</sup>) at 2 m; (b) wind speed at 10  
 789 m (green line; m s<sup>-1</sup>) and pressure (black line; hPa); (c) average PM<sub>2.5</sub> concentration (red line is  
 790 the average and the shading indicates the standard deviation; ug m<sup>-3</sup>) and ozone concentration  
 791 (blue lines and the shading indicate the standard deviation; mg m<sup>-3</sup>) of 35 environmental  
 792 monitoring stations in Beijing; (d) mixing layer height (blue line; m) and visibility (red line; km);  
 793 (e) radiation from the observation tower at 140 m, downward shortwave radiation (solid black  
 794 line; W m<sup>-2</sup>), upward shortwave radiation (dashed black line; W m<sup>-2</sup>), downward longwave  
 795 radiation (solid blue line; W m<sup>-2</sup>), upward longwave radiation (dashed blue line; W m<sup>-2</sup>), net  
 796 radiation (red line; W m<sup>-2</sup>); and (f) sensible heat flux (red line; W m<sup>-2</sup>) and latent heat flux (red  
 797 line; W m<sup>-2</sup>).



798

799

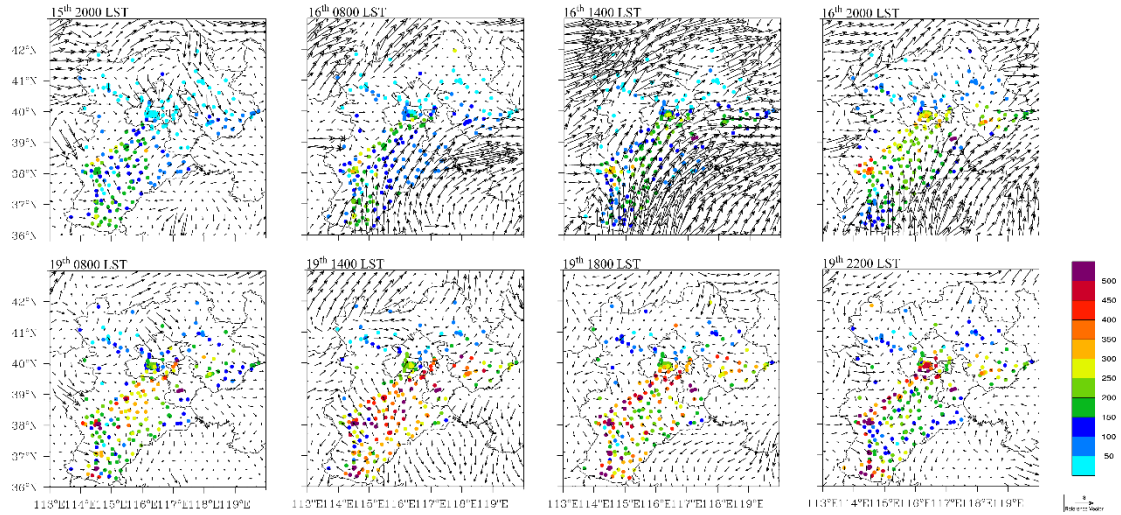
800 Figure 6 Diurnal patterns of simulated variables from the 15<sup>th</sup> to 23<sup>rd</sup> of December. (a)

801 Temperature at 2 m (°C); (b) specific humidity ( $\text{g kg}^{-1}$ ) at 2 m; (c) shortwave radiation ( $\text{W m}^{-2}$ );

802 (d) longwave radiation ( $\text{W m}^{-2}$ ); (e) MLH (m); (f) sensible heat flux ( $\text{W m}^{-2}$ ); and (g) latent heat

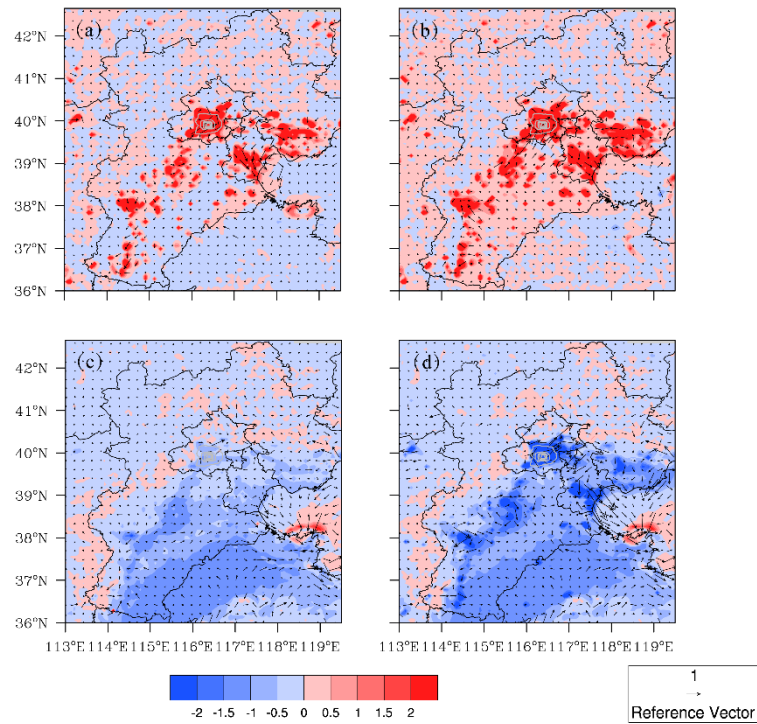
803 flux ( $\text{W m}^{-2}$ ).

804



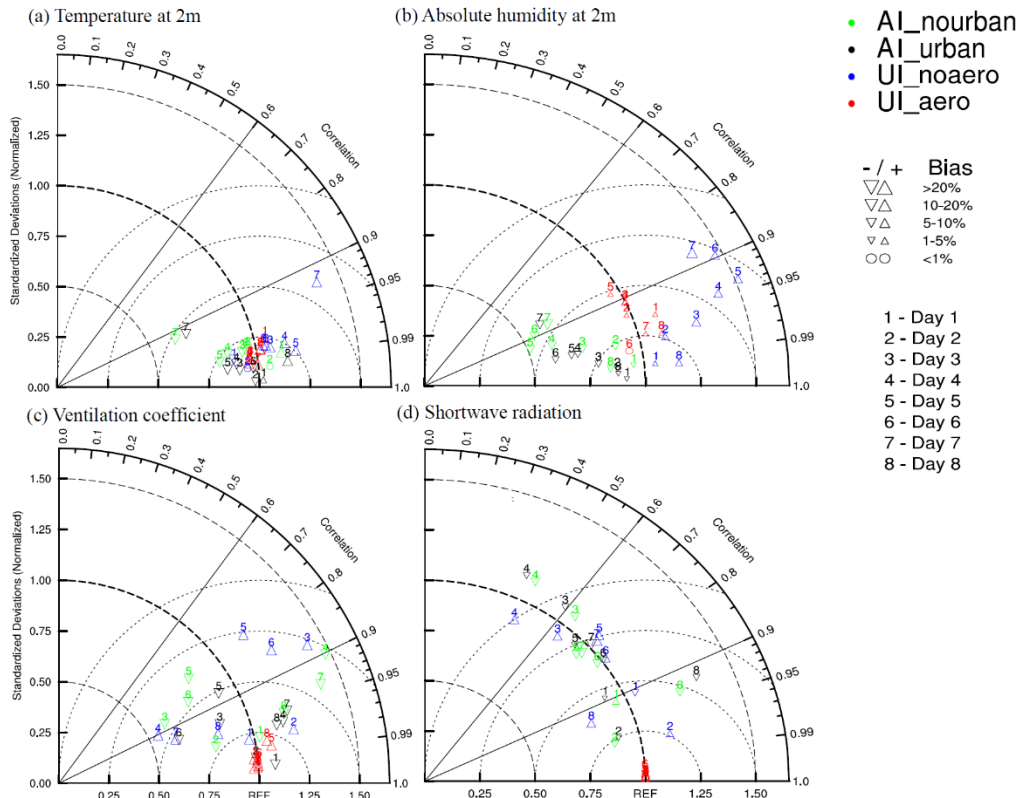
805  
806  
807  
808

Figure 7 Spatial distribution of the observed concentration of  $PM_{2.5}$  (dots;  $\mu g\ m^{-3}$ ) and wind field (vector;  $m\ s^{-1}$ ) for two increasing processes of the concentration of  $PM_{2.5}$ .



809  
810  
811  
812  
813  
814

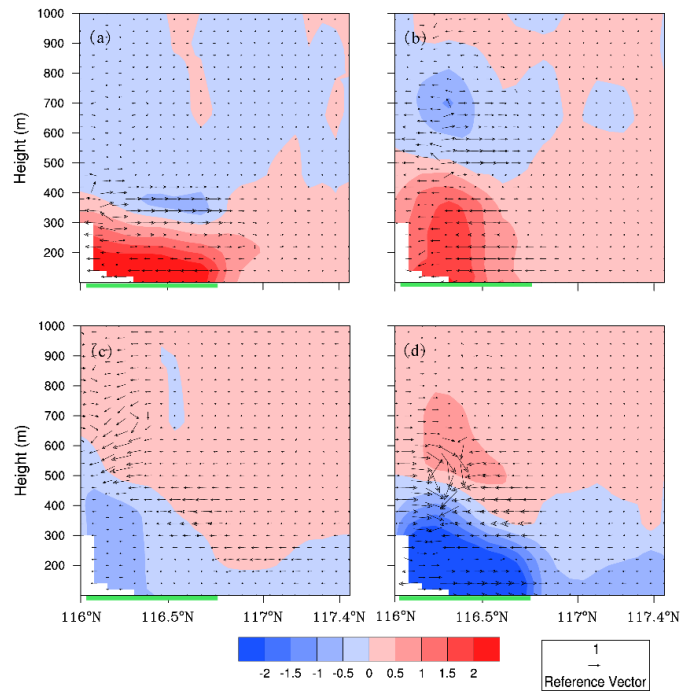
Figure 8 Spatial distribution of simulated temperature (shading;  $^{\circ}C$ ) and wind field (vector;  $m\ s^{-1}$ ). (a) UI\_aero; (b) UI\_noaero; (c) AI\_urban; (d) AI\_nourban.



815  
 816  
 817  
 818  
 819  
 820

Figure 9 Daily means of the four types of impacts (UI\_aero, UI\_noaero, AI\_urban, AI\_nourban) in the eight days are shown in Taylor diagrams in the Beijing area. (a) Temperature at 2 m ( $^{\circ}\text{C}$ ); (b) absolute humidity ( $\text{g kg}^{-1}$ ); (c) ventilation coefficient ( $\text{m}^2 \text{s}^{-1}$ ); (d) shortwave radiation ( $\text{W m}^{-2}$ ).





821  
 822  
 823  
 824  
 825  
 826  
 827  
 828  
 829  
 830  
 831  
 832  
 833

Figure 10 Cross section at 39.9°N of average temperature (shading; °C) and wind field (vector; m s<sup>-1</sup>) from 0000 LST to 0800 LST on the 16<sup>th</sup> to 20<sup>th</sup>. (a) UI\_aero; (b) UI\_noaero; (c) AI\_urban; (d) AI\_nourban.